Role of near neutron drip-line nuclei in the *r*-process*

Ting Yu (余婷)[1] Yue-Ying Guo (郭粤颖)[2,3] Xiao-fei Jiang (姜晓飞)[4] Xin-Hui Wu (吴鑫辉)[1†]

[1]Department of Physics, Fuzhou University, Fuzhou 350108, China
[2]National Astronomical Observatories, Chinese Academy of Sciences, Beijing 100101, China
[3]School of Astronomy and Space Science, University of Chinese Academy of Sciences, Beijing 100049, China
[4]State Key Laboratory of Nuclear Physics and Technology, School of Physics, Peking University, Beijing 100871, China

Abstract: The role of near neutron-drip-line nuclei in the rapid neutron-capture process (*r*-process) is studied using the classical *r*-process model. Simulations under different astrophysical conditions (T, n_n) show that *r*-process paths approach the neutron-drip line under low-temperature and high-neutron-density conditions. A sensitivity study reveals that variations in the nuclear masses of these exotic nuclei lead to evident abundance variations in the $A = 110 - 125$, $A = 175 - 185$, $A = 200 - 205$, and superheavy regions. By contrast, the *r*-process rare-earth peak and $A = 130, 195$ peaks remain largely unaffected. The nuclei that clearly impact *r*-process abundances are mainly distributed in the region of $25 \le Z \le 90$ and $50 \le N \le 180$, with the nuclei around neutron magic numbers found to be particularly important for the *r*-process, even in the near-neutron-drip-line region.

Keywords: *r*-process, near neutron drip-line nuclei, nuclear mass

DOI: 10.1088/1674-1137/ae4584 **CSTR:** 32044.14.ChinesePhysicsC.50054104

I. INTRODUCTION

The production of approximately half of the heavy elements found in nature is assigned to a specific astrophysical nucleosynthesis process: the rapid neutron-capture process (*r*-process). Although this idea was proposed approximately seven decades ago [1], a comprehensive understanding of the *r*-process remains a challenging goal owing to the difficulties encountered in both astrophysics and nuclear physics [2−6].

The astrophysical sites responsible for *r*-process abundances are still not fully understood, with some proposed scenarios still under debate. Ejecta from neutron star mergers (NSMs) is supported to be an *r*-process site from the GRB170817 kilonova [7−9] associated with gravitational waves from GW170817 [10]; however, its role in producing the *r*-process abundances observed in the oldest metal-poor stars remains debated owing to the "time delay." The neutrino driven wind (NDW) [11] and magneto-hydrodynamic jets (MHDJs) [12, 13] from core-collapse supernovae (CCSNe) and the outflows from collapsars [14−16] are favored *r*-process candidate sites that could have occurred in the early Universe. This makes them suitable for studies of nuclear cosmochronology [17−20]. However, there are debates on whether the desired high-entropy conditions for producing actinides can occur in the NDW from CCSNe [21]. The rapid time scale of the MHDJs from CCSNe and outflows from collapsars would lead to the underproduction of isotopic abundances above and below the main *r*-process peaks [5], which are different from the observed *r*-process abundances.

The *r*-process nucleosynthesis path in the nuclear chart runs to the highly neutron-rich region, on which only limited experimental information is currently available; thus, research relies heavily on theoretical predictions of nuclear properties. For extreme *r*-process astrophysical conditions with a lower electron fraction Y_e (higher neutron fraction) or lower density, the *r*-process path may even run close to the neutron-drip line, *i.e.*, the boundary of bound nuclei. Therefore, the study of exotic nuclei near the neutron-drip line is important not only for satisfying humanity's curiosity to understand exotic nuclear structures but also for understanding the origin of elements in nature. Thus, it is important to know (1) the specific astrophysical conditions under which the nuclear properties of exotic nuclei near the neutron-drip line play an important role in the *r*-process and (2) how *r*-process abundances are affected by uncertainties in the properties of these exotic nuclei.

In this study, the *r*-process conditions that lead to *r*-

Received 21 November 2025; Accepted 12 February 2026; Accepted manuscript online 13 February 2026

* Supported by the National Natural Science Foundation of China (12405134, 12435006, 12141501, 12475117), the National Key R&D Program of China (2024YFE0109803, 2024YFA1612600), the State Key Laboratory of Nuclear Physics and Technology, Peking University (NPT2023ZX03, NPT2025KFY02), and the National Key Laboratory of Neutron Science and Technology (NST202401016)

† E-mail: wuxinhui@fzu.edu.cn

process paths close to the neutron-drip line are studied using the classical *r*-process model. Under these typical conditions, the impacts of uncertainties in the nuclear masses of exotic nuclei near the neutron-drip line on *r*-process abundances are analyzed.

II. CLASSICAL *r*-PROCESS MODEL

Considering that the astrophysical sites responsible for *r*-process abundances are still not fully understood, we perform *r*-process simulations based on a site-independent *r*-process model known as the classical *r*-process model [22−27], which can be regarded as a simplification of the dynamical *r*-process model and has been successfully employed in describing *r*-process patterns of both the Solar System and metal-poor stars.

In the classical *r*-process model, iron group seed nuclei are irradiated by high-density neutron sources with a high temperature ($T \gtrsim 1.5$ GK). The *r*-process abundances are obtained via the superposition of abundances from simulations in several neutron flows with different neutron densities, temperatures, and irradiation times. The weights can be determined via fitting to the Solar *r*-process abundances.

In astrophysical environments with high-temperatures ($T \gtrsim 1.5$ GK) and high neutron densities ($n_n \gtrsim 10^{20}$ cm^{-3}), equilibrium between neutron capture and photodisintegration reactions can be achieved, and the abundance ratios of neighboring isotopes on an isotopic chain can be obtained using the Saha equation [2, 28, 29],

$$\frac{Y(Z,A+1)}{Y(Z,A)} = n_n \left(\frac{2\pi\hbar^2}{m_\mu kT}\right)^{3/2} \frac{G(Z,A+1)}{2G(Z,A)} \left(\frac{A+1}{A}\right)^{3/2} \times \exp\left[\frac{S_n(Z,A+1)}{kT}\right], \quad (1)$$

where $Y(Z,A), S_n(Z,A)$, and $G(Z,A)$ are the abundance, one-neutron separation energy, and partition function of nuclide (Z,A), respectively, and $\hbar$, k, and m_μ are the Planck constant, Boltzmann constant, and atomic mass unit, respectively. Note that the neutron separation energy S_n deduced from nuclear masses appears in the exponential, suggesting the importance of nuclear mass in such equilibrium. In the classical *r*-process model, the *r*-process path is defined as the path that traverses the most abundantly distributed nucleus in each isotopic chain, as determined by Eq. (1).

The abundance flow from one isotopic chain to the next is governed by β decays and can be expressed by a set of differential equations

$$\frac{\mathrm{d}Y(Z)}{\mathrm{d}t} = Y(Z-1)\sum_A P(Z-1,A)\lambda_\beta^{Z-1,A} - Y(Z)\sum_A P(Z,A)\lambda_\beta^{Z,A}, \quad (2)$$

where $\lambda_\beta^{Z,A}$ is the β-decay rate of nucleus (Z,A), $Y(Z) = \sum_A Y(Z,A) = \sum_A P(Z,A)Y(Z)$ is the total abundance of each isotopic chain, and $P(Z,A)$ denotes the individual population coefficients. The abundance of each isotope can be determined using Eqs. (1) and (2). After the neutrons freeze-out, unstable isotopes on the neutron-rich side proceed to stable isotopes mainly via β decays, and the final abundances are obtained.

The nuclear physics inputs for the classical *r*-process model include nuclear masses and β-decay half lives. The nuclear masses are taken from the WS4 nuclear mass model [30] if experimental data [31] are not available. For the β-decay rates, the empirical formula [32] is used with decay energies from the adopted nuclear masses if experimental data [33] are not available.

III. *r*-PROCESS CONDITIONS FOR YIELDING NEUTRON-DRIP-LINE *r*-PROCESS PATHS

The first step is to identify the astrophysical conditions that bring the *r*-process nucleosynthesis paths close to the neutron-drip line. *r*-process paths under different astrophysical conditions (T, n_n) are presented in Fig. 1. As shown, the paths are closer to the neutron-drip line at both higher neutron densities n_n and lower temperatures T. This can be easily understood via Eq. (1), as both a higher neutron density n_n and lower temperature T lead to a larger ratio of $Y(Z,A+1)/Y(Z,A)$, thus leading to a more extensive abundance distribution on the neutron-rich side, *i.e.*, *r*-process paths shift toward the neutron-rich region.

The *r*-process abundances corresponding to different sets of astrophysical conditions (neutron number density n_n; temperature T) and a fixed irradiation time of $\tau = 850$ ms are presented in Fig. 2. As neutron density increases and temperature decreases, the *r*-process abundance distribution shifts toward the region of heavier nuclides. This may indicate that the properties of near-neutron-drip-line nuclei are likely to be more important for determining the *r*-process abundances of heavier nuclides.

To quantitatively determine the relationship between the proximity of *r*-process paths to the neutron-drip line and astrophysical conditions, the average distance between an *r*-process path and the neutron-drip line is investigated, which is defined as follows:

$$L = \frac{1}{Z_f - Z_i}\sum_{Z=Z_i}^{Z_f}[N_d(Z) - N_r(Z)], \quad (3)$$

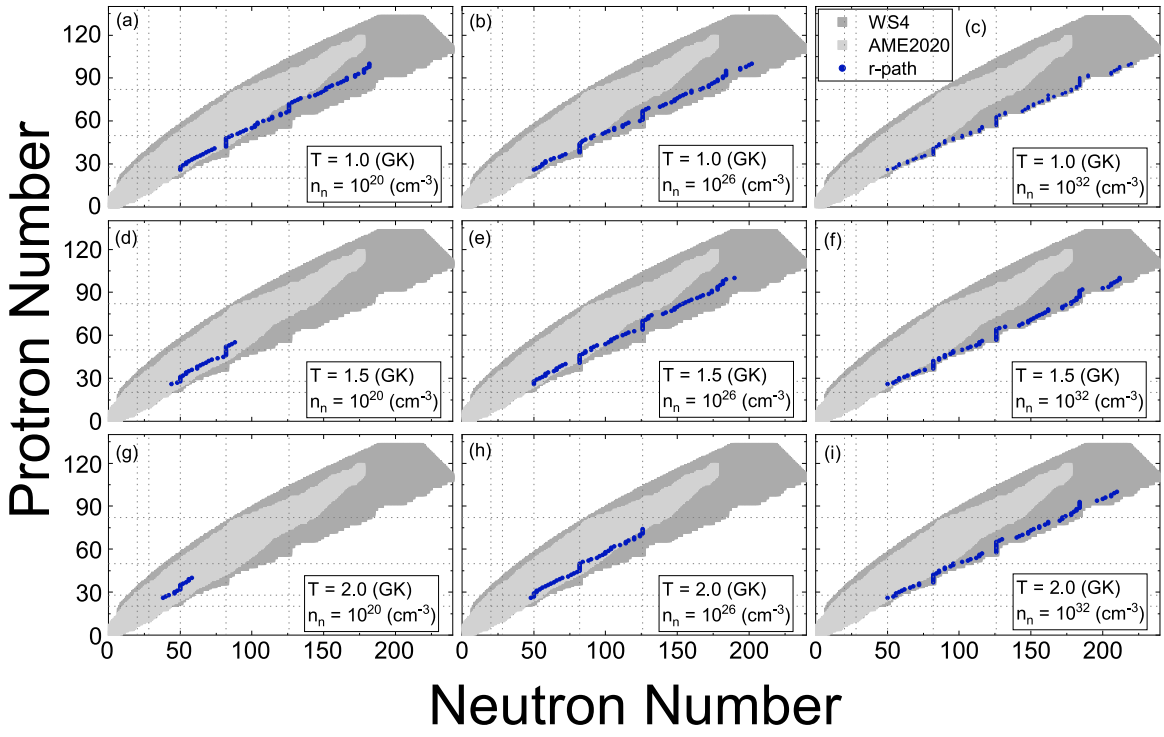

Fig. 1. (color online) *r*-process nucleosynthesis paths under different astrophysical conditions, characterized by temperature (T) and neutron number density (n_n).

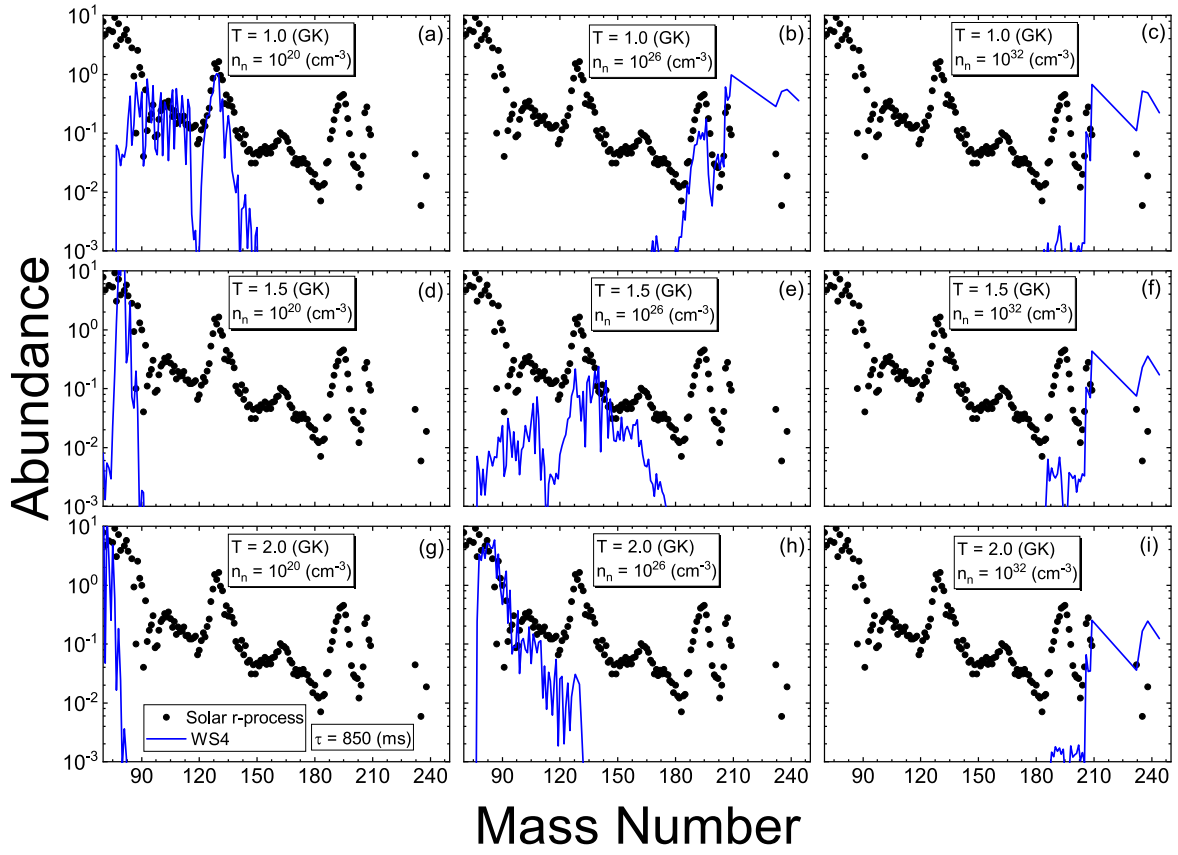

Fig. 2. (color online) *r*-process abundances under different astrophysical conditions, characterized by temperature (T) and neutron number density (n_n), with a fixed irradiation time of $\tau = 850$ ms.

where $N_d(Z)$ and $N_r(Z)$ are the neutron numbers of the neutron-drip-line and *r*-process path nuclei in the isotopic chain of a given proton number Z, respectively. Z_i and Z_f are the chosen initial and final proton numbers along the *r*-process path, which define a specific segment of the *r*-process path. Note that each *r*-process path nucleus is characterized by a specific (Z,N) pair; therefore, Z_i (Z_f) also corresponds to a specific N_i (N_f). The smaller the distance L, the closer the *r*-process path is to the neutron-drip line. When $L=0$, the *r*-process path lies directly on the neutron-drip line, a scenario that corresponds to extremely neutron-rich astrophysical conditions.

The averaged distances between *r*-process paths and the neutron-drip line under different astrophysical conditions are illustrated in Fig. 3. Each *r*-process path is separated into three segments: $N \le 82$ for light nuclei, $82 \le N \le 126$ for medium nuclei, and $N \ge 126$ for heavy nuclei. As shown in Fig. 3, the distance L decreases monotonically as neutron density increases and temperature decreases, and the *r*-process paths reach the neutron-drip line when the neutron density and temperature reach certain values. In the region of light nuclei, the *r*-process paths can get relatively closer to the neutron-drip line under lower neutron density and higher temperature conditions. This is because the neutron-drip line does not extend as far in the lighter nuclear region as in the heavier nuclear region.

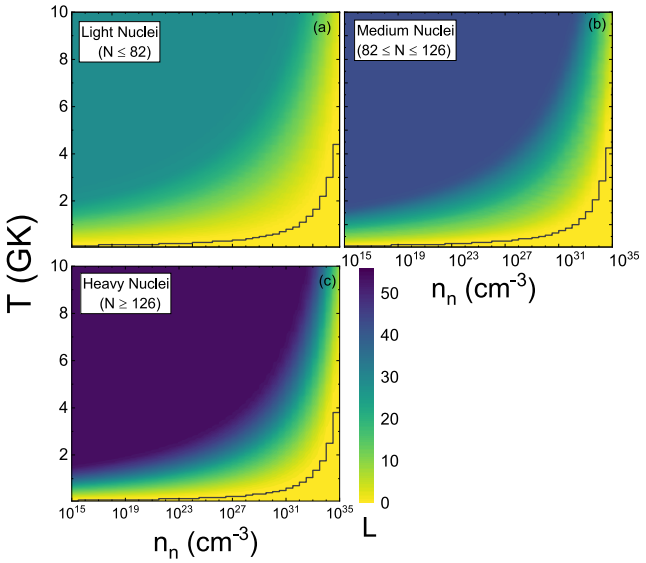

Fig. 3. (color online) Averaged distances between *r*-process paths and the neutron-drip line under different astrophysical conditions, characterized by neutron number density n_n and temperature T. Each *r*-process path is divided into three segments based on neutron number N: $N \le 82$ (light nuclei), $82 \le N \le 126$ (medium nuclei), and $N \ge 126$ (heavy nuclei). The black lines denote the astrophysical conditions that first enable the *r*-process paths to reach the neutron-drip line.

IV. IMPACT OF NEAR-NEUTRON-DRIP-LINE NUCLEI ON *R*-PROCESS ABUNDANCES

The next step is to examine the impacts of the nuclear properties of near-neutron-drip-line nuclei on the *r*-process. For this purpose, a sensitivity study similar to that reported in Refs. [27, 34, 35] is conducted.

Four sets of *r*-process simulations under astrophysical conditions with neutron number densities of $n_n = 10^{25}$ cm^{-3}, $n_n = 10^{27}$ cm^{-3}, $n_n = 10^{28}$ cm^{-3}, and $n_n = 10^{30}$ cm^{-3} and a fixed irradiation time $\tau = 850$ ms and temperature $T = 1.5$ GK are selected as typical cases that represent astrophysical conditions corresponding to the abundances of different mass regions. *r*-process simulations under these conditions and unvaried nuclear physics inputs are regarded as baseline simulations. Note that the astrophysical conditions adopted in this study are relatively extreme, which is intended to bring the *r*-process path close to the neutron-drip line. Nevertheless, these conditions remain reasonable and fall within the scope of certain parameterized environments for supernova explosions [36] and NSMs [37] in dynamic *r*-process studies. The *r*-process paths and abundances corresponding to these four sets of astrophysical conditions are presented in Fig. 4. As shown in Fig. 4 (a), the *r*-process paths of these four cases under the selected conditions are generally close to the neutron-drip line. Note that, in addition

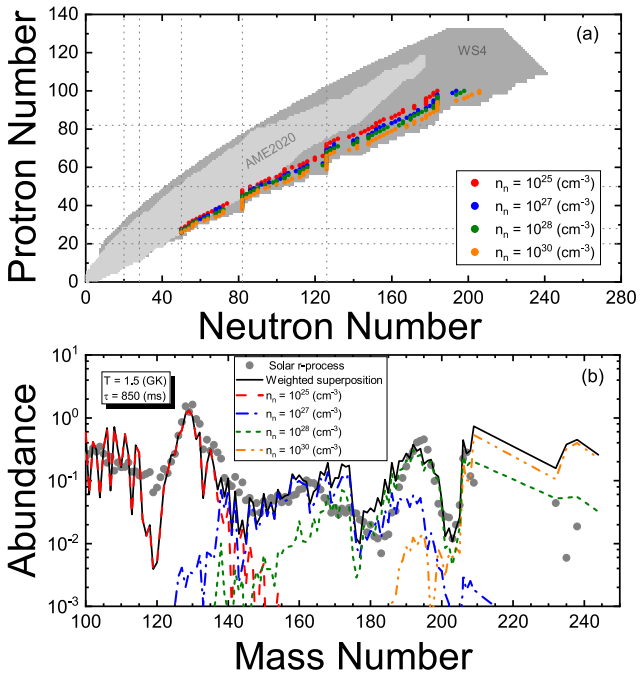

Fig. 4. (color online) (a) *r*-process paths and (b) *r*-process abundances under four typical sets of astrophysical conditions. The neutron number densities are $n_n = 10^{25}$ cm^{-3}, $n_n = 10^{27}$ cm^{-3}, $n_n = 10^{28}$ cm^{-3}, and $n_n = 10^{30}$ cm^{-3}, with fixed irradiation time $\tau = 850$ ms and temperature $T = 1.5$ GK.

to the nuclei on the *r*-process paths, those close to the *r*-process path affect the r-process abundances to varying extents. In this regard, the properties of near-neutron-drip-line nuclei could, in principle, affect the results of all four sets of simulations. The *r*-process simulations under the four cases correspond to the abundances of the $A \sim 130$ peak, rare-earth isotopes, $A \sim 195$ peak, and superheavy radioactive nuclei, respectively. This will be helpful when analyzing the effect of the properties of near-neutron-drip-line nuclei on the *r*-process abundances of nuclei in different mass regions. As shown in Fig. 4 (b), the weighted superposition of these four sets of *r*-process abundances can reproduce the Solar *r*-process abundances well. Therefore, the current sets of simulations represent reasonably realistic scenarios that *r*-process studies can use to reproduce the observed *r*-process abundance.

To perform a sensitivity study on how nuclei near the neutron-drip line affect *r*-process abundances, the following steps are implemented: First, the neutron-rich nuclei in each isotopic chain are classified into different sets according to their distances relative to the neutron-drip nucleus of that isotopic chain. Figure 5 shows the collections of nuclei in Set 1, Sets 1 to 5, Sets 1 to 10, and Sets 1 to 20. A sensitivity study is then performed by varying each predicted nuclear mass in these collections (for different numbers of sets of nuclei) with $\Delta M = \pm 0.5$ MeV in the *r*-process simulations. Note that only the upper and lower bounds of the nuclear mass variations are considered. The β-decay half lives are varied consistently with the mass variations by imposing different Q_β values in the empirical formula [32]. Subsequently, a number of resultant *r*-process abundance patterns are obtained, which form a band as shown in each subplot of Fig. 6.

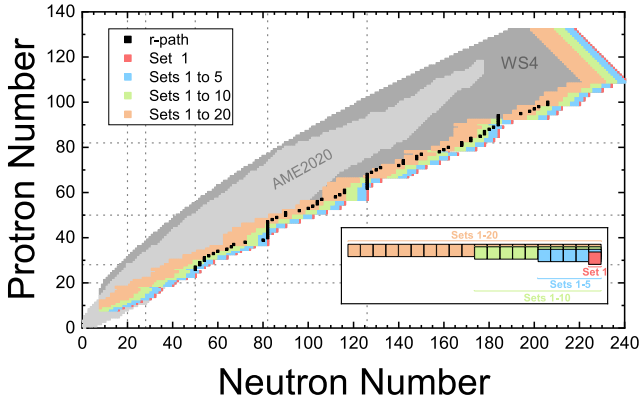

Fig. 5. (color online) Illustrations of the different nuclear collections varied in the sensitivity study: Set 1, Sets 1 to 5, Sets 1 to 10, and Sets 1 to 20. Each collection consists of neutron-rich nuclei classified by their distance relative to the neutron-drip line of their respective isotopic chains. The *r*-process path is obtained via weighted superposition of the four paths shown in Fig. 4 (a). The inset subplot shows the detailed partitioning of the 20 most neutron-rich nuclei in each isotope chain into each collection.

As shown in Fig. 6, variations in the nuclear masses of near-neutron-drip-line nuclei can directly lead to significant variations in the abundances of superheavy nuclei, such as lead and actinide nuclei. The abundances of these nuclei are mainly produced under the astrophysical condi-

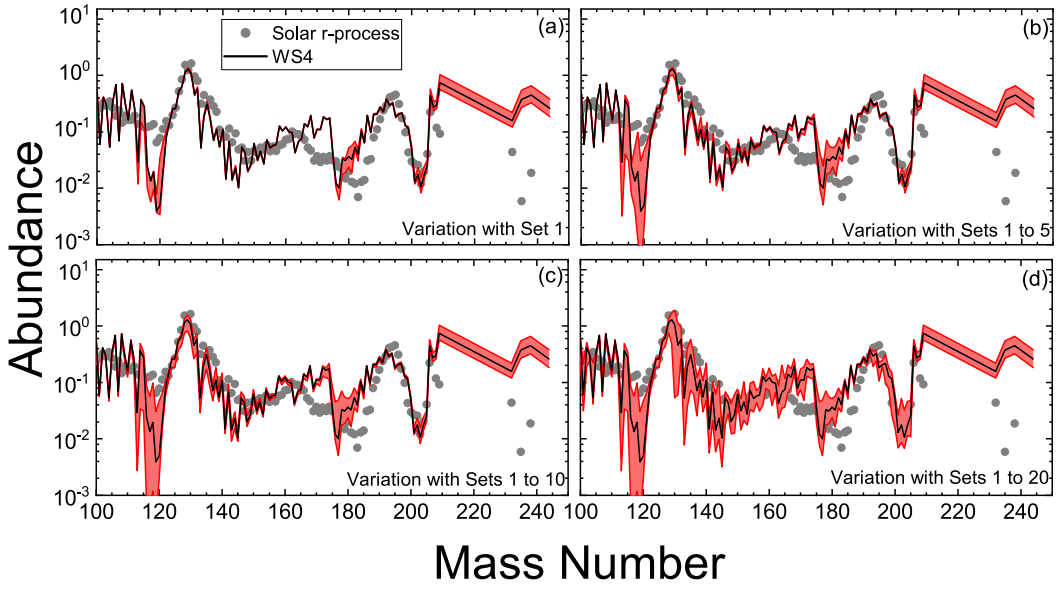

Fig. 6. (color online) Variations in *r*-process abundances corresponding to the nuclear mass variations in the sensitivity study. Each subplot corresponds to the nuclear collection illustrated in the matching collection in Fig. 5: (a) variations for Set 1 nuclei, (b) variations for Sets 1 to 5 nuclei, (c) variations for Sets 1 to 10 nuclei, and (d) variations for Sets 1 to 20 nuclei. The bands in each subplot represent the range of abundance variations caused by $\Delta M = \pm 0.5$ MeV nuclear mass variations.

tion with $n_n = 10^{30}$ cm^{-3} (see Fig. 4 (b)), and the *r*-process path associated with this condition is mostly close to the neutron-drip line, as shown in Fig. 4 (a).

Fig. 6 also shows that variations in abundance are evident in regions with $A = 110-125$, $A = 175-185$, and $A = 200-205$, directly before their respective abundance peaks. The reasons for the variations with $A = 110-125$ and $A = 175-185$ are the same. The first reason arises from differences in abundance magnitudes between these nuclei and the peak nuclei. The abundances of these nuclei are smaller by more than one order of magnitude compared with the peak abundances; therefore, even small variations in the abundances of peak nuclei can lead to significant variations in the abundances of these nuclei. This reasoning also applies to the $A = 200-205$ region. The second reason involves neutron shell effects across different isotopic chains. For example, the *r*-process path nuclei associated with the $N = 82$ neutron shell holds for isotope chains with $Z = 40-47$. The abundances accumulated in these nuclei contribute to those of nuclei in and around the $A = 130$ *r*-process peak. Because nuclei with smaller Z (*e.g.*, $Z = 40$) are closer to the neutron-drip line, they are affected more significantly than the others in the sensitivity study. This leads to larger abundance variations in nuclei with $A = 122$ and below, owing to β-decay neutron emissions, which causes the abundance variations in the $A = 110-125$ region. Similar mechanisms also cause the evident abundance variations in the $A = 175-185$ region, which relate to the $N = 126$ neutron shell. Another reason for the nuclear mass variations in the $A = 200-205$ region is the same as that for lead and actinide nuclei: the corresponding *r*-process path is closest to the neutron-drip line.

One important indication is that the abundances of lanthanide nuclides, especially those in the *r*-process rare-earth peak, are affected only when the number of variation sets reaches 20. This is good news for studies that aim to understand the origin of the rare-earth peak, as it may not be strongly affected by the large uncertainties of nuclei close to the neutron-drip line. Furthermore, the *r*-process peaks at $A = 130$ and $A = 195$ are not affected by variations in the nuclear masses of nuclei close to the neutron-drip line. This is reasonable, as it is well known that *r*-process simulations based on different nuclear mass models, even those that differ in the locations of the neutron-drip line, consistently yield these two *r*-process peaks.

Moreover, the nuclei near the neutron-drip line that are important for the *r*-process abundances should be identified. To quantify the abundance variations caused by varying the mass of each nucleus, the abundance deviation ΔY is introduced:

$$\Delta Y = \frac{1}{N}\sum_{A=100}^{244} |\log Y_{\max}(A) - \log Y_{\min}(A)|, \tag{4}$$

where $Y_{\max}(A)$ ($Y_{\min}(A)$) is the largest (smallest) abundance obtained from *r*-process simulations with baseline inputs, baseline inputs with $\Delta M = +0.5$ MeV for a specific nucleus, and baseline inputs with $\Delta M = -0.5$ MeV for that nucleus.

The *r*-process abundance deviations caused by varying the mass of each single nucleus are presented in Fig. 7. As shown in Fig. 7 (a), the nuclei that clearly impact *r*-process abundances are mainly distributed in the region of $25 \le Z \le 90$ and $50 \le N \le 180$. In the classical *r*-process model, iron is used as the seed nucleus; hence, lighter nuclei are ignored. It is encouraging to find that nuclei heavier than $A = 270$ cause relatively small uncertainties in *r*-process abundances; otherwise, one such nucleus could lead to large uncertainties in understanding the *r*-process, as there are still significant uncertainties in theoretically describing these heavy neutron-rich nuclei. However, this could also be because fission is not included in the classical *r*-process model employed in this study. The masses of $A > 270$ nuclei can affect their fission rates, which in turn can influence *r*-process abundances. As clearly shown in Fig. 7 (b), when varying the

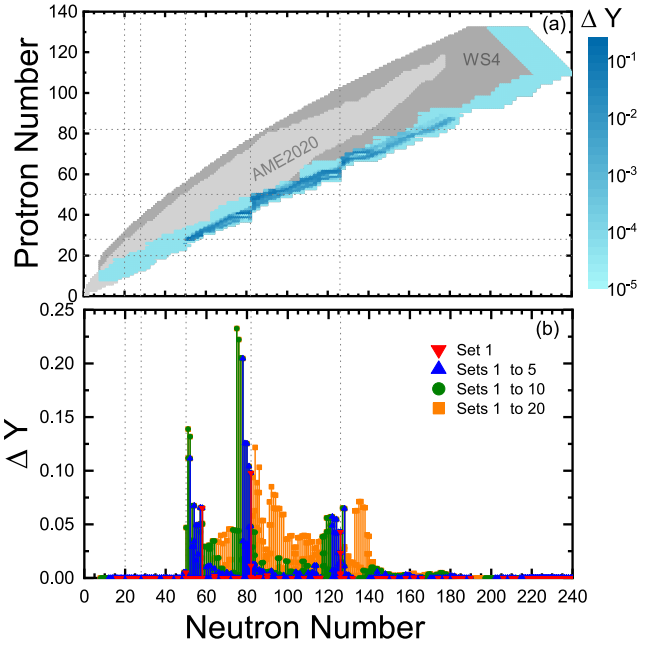

Fig. 7. (color online) (a) Nuclear chart presenting the *r*-process abundance deviations ΔY caused by varying nuclear mass of each single nucleus. (b) The abundance deviations ΔY are plotted as a function of neutron number to have a clear visualization with colors label nuclei in different sets. Note that panel (b) is just another representation of ΔY in panel (a); it does not sum over ΔY caused by nuclei with the same N.

masses of nuclei from set 1 (neutron-drip line nuclei) to set 20 (neutron-rich nuclei), the nuclei that significantly impact r-process abundances first appear around the neutron magic numbers $N=50$ with $Z\approx 28$, $N=82$ with $Z\approx 41$, and $N=126$ with $Z\approx 66$. This then extends to other regions, mainly those around rare-earth isotopes. This indicates that nuclei around neutron magic numbers are important for the *r*-process, even in the near-neutron-line region. Note that a large deviation can be observed between $N=82$ and $N=126$ in Fig. 7 (b), which is related to the lanthanide region. This region is of great interest in both nuclear physics and astrophysics because it is the nuclear shape-transition region, and the origin of the rare-earth *r*-process abundance peak in this region remains unresolved [38, 39]. Because the deviation is significant for Sets 11 to 20, a more accurate description of nuclei located over a dozen nucleons from the drip line is required to reveal the origin of rare-earth *r*-process abundance.

V. SUMMARY

In summary, the role of near-neutron-drip-line nuclei in the *r*-process is studied using the classical *r*-process model. By performing *r*-process simulations under different astrophysical conditions (T, n_n), lower temperatures and higher neutron densities are found to drive *r*-process paths to approach the neutron-drip line and shift abundance distributions toward heavier nuclides. Quantitatively, the distance between the *r*-process path and neutron-drip line decreases monotonically with increasing neutron density and decreasing temperature across all mass regions.

A weighted superposition of four sets of *r*-process simulations under different neutron number densities reproduces Solar *r*-process abundances reasonably well. Based on this baseline, a sensitivity study further demonstrates that variations in the nuclear masses of near-neutron-drip-line nuclei significantly impact the abundances of superheavy nuclei and lead to obvious abundance variations in the $A=110-125$, $A=175-185$, and $A=200-205$ regions. By contrast, the *r*-process rare-earth peak and $A=130, 195$ peaks remain largely unaffected. The nuclei that clearly impact *r*-process abundances are mainly distributed in the region of $25\le Z\le 90$ and $50\le N\le 180$, with the nuclei around neutron magic numbers found to be particularly important for the *r*-process, even in the near-neutron-drip-line region.

These results highlight the need for precise constraints on the properties of near-neutron-drip-line nuclei to advance our understanding of *r*-process nucleosynthesis.

References

[1] E. M. Burbidge, G. R. Burbidge, W. A. Fowler *et al.*, Rev. Mod. Phys. **29**(4), 547 (1957)
[2] M. Arnould, S. Goriely, K. Takahashi, Phys. Rep. **450**, 97 (2007)
[3] F.-K. Thielemann, A. Arcones, R. Käppeli *et al.*, Prog. Part. Nucl. Phys. **66**, 346 (2011)
[4] F.-K. Thielemann, M. Eichler, I. Panov *et al.*, Annu. Rev. Nucl. Part. Sci. **67**, 253 (2017)
[5] T. Kajino, W. Aoki, A. Balantekin *et al.*, Prog. Part. Nucl. Phys. **107**, 109 (2019)
[6] J. J. Cowan, C. Sneden, J. E. Lawler *et al.*, Rev. Mod. Phys. **93**(1), 015002 (2021)
[7] B. P. Abbott, R. Abbott, T. D. Abbott *et al.*, Astrophys. J. **848**, L12 (2017)
[8] E. Pian, P. D'Avanzo, S. Benetti *et al.*, Nature **551**, 67 (2017)
[9] D. Watson, C. J. Hansen, J. Selsing *et al.*, Nature **574**, 497 (2019)
[10] B. P. Abbott, R. Abbott, T. D. Abbott *et al.* (LIGO Scientific Collaboration and Virgo Collaboration), Phys. Rev. Lett. **119**, 161101 (2017)
[11] S. E. Woosley, J. R. Wilson, G. J. Mathews *et al.*, Astrophys. J. **433**, 229 (1994)
[12] N. Nishimura, T. Takiwaki, F.-K. Thielemann, Astrophys. J. **810**, 109 (2015)
[13] N. Nishimura, T. Kajino, G. J. Mathews *et al.*, Phys. Rev. C **85**, 048801 (2012)
[14] D. M. Siegel, J. Barnes, B. D. Metzger, Nature **569**, 241 (2019)
[15] K. Nakamura, T. Kajino, G. J. Mathews *et al.*, Astron. Astrophys. **582**, A34 (2015)
[16] M. Famiano, A. B. Balantekin, T. Kajino *et al.*, Astrophys. J. **898**, 163 (2020)
[17] V. Hill, N. Christlieb, T. C. Beers *et al.*, Astron. Astrophys. **607**, A91 (2017)
[18] X. H. Wu, P. W. Zhao, S. Q. Zhang *et al.*, Astrophys. J. **941**, 152 (2022)
[19] X.-H. Wu, J. Meng, Sci. Bull. **68**, 539 (2023)
[20] Y. Y. Huang, Q. Q. Cui, X. H. Wu *et al.*, Astrophys. J. **988**, 22 (2025)
[21] T. Fischer, S. C. Whitehouse, A. Mezzacappa *et al.*, Astron. Astrophys. **517**, A80 (2010)
[22] K.-L. Kratz, J.-P. Bitouzet, F.-K. Thielemann *et al.*, Astrophys. J. **403**, 216 (1993)
[23] K.-L. Kratz, K. Farouqi, B. Pfeiffer *et al.*, Astrophys. J **662**, 39 (2007)
[24] B. Sun, F. Montes, L. S. Geng *et al.*, Phys. Rev. C **78**, 025806 (2008)
[25] X. D. Xu, B. Sun, Z. M. Niu *et al.*, Phys. Rev. C **87**, 015805 (2013)
[26] B. Zhao, S. Q. Zhang, Astrophys. J. **874**, 5 (2019)
[27] X. F. Jiang, X. H. Wu, P. W. Zhao, Astrophys. J. **915**, 29 (2021)
[28] J. J. Cowan, F.-K. Thielemann, J. W. Truran, Phys. Rep. **208**, 267 (1991)
[29] Y.-Z. Qian, Prog. Part. Nucl. Phys. **50**, 153 (2003)
[30] N. Wang, M. Liu, X. Wu *et al.*, Phys. Lett. B **734**, 215 (2014)

[31] M. Wang, W. Huang, F. Kondev *et al.*, Chin. Phys. C **45**, 030003 (2021)
[32] Y. Zhou, Z. Li, Y. Wang *et al.*, Sci. China-Phys. Mech. Astron. **60**, 082012 (2017)
[33] M. Chadwick, P. Obložinský, M. Herman *et al.*, Nuclear Data Sheets **107**, 2931 (2006)
[34] M. R. Mumpower, R. Surman, D.-L. Fang *et al.*, Phys. Rev. C **92**, 035807 (2015)
[35] M. Mumpower, R. Surman, G. McLaughlin *et al.*, Prog. Part. Nucl. Phys. **86**, 86 (2016)
[36] K. Farouqi, K.-L. Kratz, B. Pfeiffer *et al.*, Astrophys. J. **712**, 1359 (2010)
[37] J. Lippuner, L. F. Roberts, Astrophys. J. **815**, 82 (2015)
[38] R. Surman, J. Engel, J. R. Bennett *et al.*, Phys. Rev. Lett. **79**, 1809 (1997)
[39] S. Goriely, J.-L. Sida, J.-F. Lemaître *et al.*, Phys. Rev. Lett. **111**, 242502 (2013)